International Journal on Magnetic Particle Imaging
Vol 8, No 1, Suppl 1, Article ID 2203065, 4 Pages

Infinite Science Publishing

Proceedings Article

Low-Power Iron Selection and Focus Field Generator

Fynn Foerger [1,2,*] · Marija Boberg [1,2] · Martin Möddel [1,2] · Jan-Philipp Scheel [2] · Matthias Graeser [1,2,3,4] · Tobias Knopp [1,2]

[1] Section for Biomedical Imaging, University Medical Center Hamburg-Eppendorf, Hamburg, Germany
[2] Institute for Biomedical Imaging, Hamburg University of Technology, Hamburg, Germany
[3] Fraunhofer Research Institute for Individualized and Cell-based Medicine, Lübeck, Germany
[4] Institute for Medical Engineering, University of Lübeck, Lübeck, Germany
[*] Corresponding author, email: f.foerger@uke.de

Abstract

A major issue for human-sized Magnetic Particle Imaging scanners is the generation of sufficiently large magnetic gradient fields. By taking advantage of the field amplification properties of soft-iron, a considerable amount of power can be saved. In this work, an optimized selection and focus field generator is presented, that can generate flexible and high gradient fields at comparatively low power consumption. Coil spacing and possible field-free-point positions are similar to conventional MPI scanners designed with air coils, but with significantly less demands on infrastructure and cooling design. The optimization process is discussed and first field measurements are presented.

I. Introduction

In most Magnetic Particle Imaging (MPI) scanners a major part of the required power is used to generate selection and focus fields (SeFo). On the way to a human-sized MPI scanner, power efficient SeFo generators are crucial [1–4]. Air coils are no longer feasible above a certain bore size, due to power limitations. For this reason, soft iron or permanent magnets are the means of choice for field amplification in the low and medium frequency range [5, 6]. Both can drastically reduce the power required and have their advantages and disadvantages. For example, the field simulation effort for soft-iron is strongly increased compared to air coils, whereas adjustable magnetic fields using permanent magnets are only realizable with high mechanical effort.

In this work, an optimized field-free-point magnetic field generator with multiple iron-core coils is designed and built. The design allows production of high, flexible and switchable magnetic fields with low mechanical effort. In particular, three-dimensional FFP movements are possible. Thus, imaging and magnetic manipulation experiments [7, 8] can be performed with high gradients, short sequence times and easy access to the system. Additionally, the nonlinear inverse current problem can be studied in detail [9]. This includes calculating the current for a desired field configuration under influence of the nonlinear response of the iron magnetization.

In this paper, the main aspects of the design process including the geometry optimization are explained and first field measurements are presented validating the performed simulations. Additionally, further simulations concerning the power consumption of the system for different field free points (FFP) are shown.

II. Methods

To optimize an iron coil setup one has to find an efficient current density and iron distribution. By adapting the geometry and material parameters for the specific application, a considerable amount of power can be saved. In this study, optimization simulations are performed with

the COMSOL Multiphysics software[1], which provides a toolbox for solving differential equations using the finite element method (FEM).

We start with the generator optimization and a fit of the simulated field to the measured field by using a free parameter. Afterwards, the simulation method for the power consumption of the system follows.

II.I. Field Generator Optimization

The number of degrees of freedom in a geometry optimization is high. Thus, it is important to choose a certain design concept in advance, in which the optimization parameters can be defined. Therefore, it is useful to consider physical aspects like demagnetization factors or the course of the field lines.

The array shaped coil assembly design (Figure 1) presented here was first optimized for human head imaging and later scaled down by factor of three for prototyping. This results in a coil spacing of 10 cm and reachable FFP positions in a $10 \times 8 \times 10\,\mathrm{cm}^3$ volume. But consequently, the main constraints of the large setup are still reflected in the geometry of the down scaled version. For example, coils are only placed on two sides.

In order to capture the saturation properties in the simulation, the magnetization curve of soft-iron from COMSOLs material library is used. For the objective function, the overall power consumption for a central FFP with a gradient strength of $2.0\,\mathrm{Tm}^{-1}$ is defined such that the iron is saturated during operation. Geometry optimization parameters are the number of coils per side, the coil length, the coil cross section and the core size. Further, the width of the outer iron coating is included in the optimization, which serves to guide the field lines into the area of interest. Additionally, the current density is allowed to vary along the iron cores. For this purpose, the coil is divided into four different areas with constant current density. Depending on the connection of these elements, different current density distributions can be achieved. The one with the highest efficiency for high field strengths is selected.

For optimization, COMSOLs Optimization Module is used, offering a wide variety of optimization algorithms. Here, a Nelder-Mead algorithm is applied.

II.II. Verification

In the best case, simulations should reflect the real world. However, it is impossible to include all aspects in a simulation from the beginning. For example, the fill factor η (proportion of copper in the cross section of the coil) is not known in advance or imperfections in the iron assembly could exist. For this reason, η is left as a free parameter to fit the measured data to the simulated data. The simulation can be considered to be a valid approximation when the field profile and its dependence on the current density is properly reflected.

To determine η, only the center coil of each coil cage is inserted (see Figure 1) and supplied with low current, such that saturation does not play a role and there is a linear relationship between η and the field values. Thereupon, $\partial_y B_y$ is selected as a representative for the field values and used to scale the fill factor. In order to measure $\partial_y B_y$, a compact polynomial representation using spherical harmonics as introduced in [10] is chosen. Only 86 measurement points of a spherical 12-design are necessary to obtain a polynomial of degree 6.

Afterwards, a simulation is performed with the same current and $\eta = 1$. The actual fill factor results in $\eta = \left(\partial_y B_y\right)_\mathrm{M} / \left(\partial_y B_y\right)_\mathrm{S}$ (M: Measurement, S: Simulation). Afterwards field measurements and simulations atcd higher current densities can be compared to assess whether the saturation properties of the iron are being accurately simulated and the field profiles of the measurement and the simulation stay consistent.

II.III. Power Consumption Simulation

With the previously determined η, further simulations can be done concerning the power consumption of the system when all coils are inserted. The needed currents for an FFP at a specific position are calculated by performing a gradient based optimization with an algorithm implemented in COMSOL. Thereby, the currents are varied under certain boundary conditions such that the FFP is in the right place and the desired field profile is achieved. From the currents the power consumption of the system is determined. Here, FFP positions are considered which lie on the y-axis between both coil arrays. The Jacobian Matrix, as a local representation of the field in the FFP, is set to

$$\boldsymbol{J} = \begin{pmatrix} -G/2 & 0 & 0 \\ 0 & G & 0 \\ 0 & 0 & -G/2 \end{pmatrix}$$

with $G = 1.5\,\mathrm{Tm}^{-1}$.

III. Results and Discussion

The optimization process yields a setup with nine coils per side, a gradient strength of $1.5\,\mathrm{T\,m}^{-1}$ and an overall power consumption of 210 W for a central FFP. A photo and a schematic rendering of the setup is shown in Figure 1. Due to the long soft-iron cores, the coil length and the current density distribution can still be optimized during build up. When using another material like cobalt-iron (CoFe) for the cores and the outer coating, an even lower power consumption can be expected. This is due to the

[1] COMSOL Multiphysics® v. 5.6. www.comsol.com. COMSOL AB, Stockholm, Sweden.

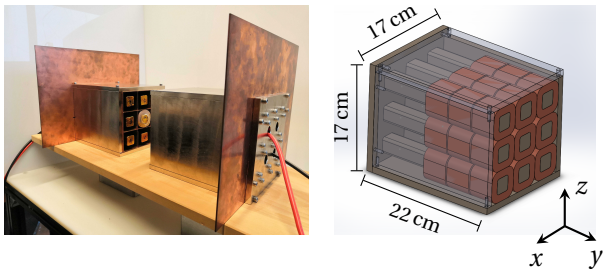

Figure 1: Photo of the field generator when the middle coil is inserted and schematic rendering of a single coil cage with $3 \times 3\,\mathrm{c}^2$oils. The dimensions of the individual coils are $5 \times 5 \times 15\,\mathrm{cm}^3$. Each coil consists of individual coil segments and each segment is made from a copper strip wound on the respective iron core. The supply cables are led out of the iron back plate. The copper plates inside the iron block visible on the photo on the left, serve on the one hand for positioning the coils and on the other hand for additional heat dissipation. On the right side, copper colored elements are the field-generating coils mounted on the gray colored soft-iron.

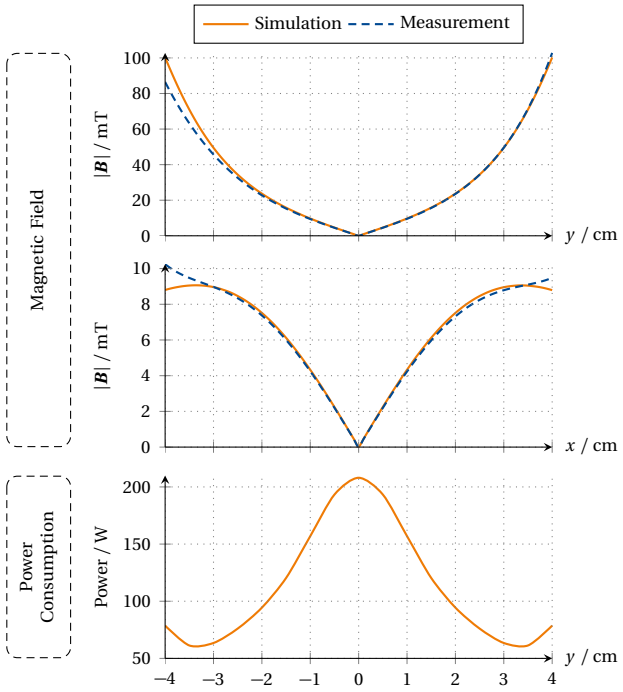

Figure 2: Simulated and measured magnetic flux density $\boldsymbol{B}$ and power consumption for FFP movement on y-axis with $G = 1.5\,\mathrm{Tm}^{-1}$.

fact that the saturation magnetization of CoFe is 2.35 T compared to 2.15 T for high-purity soft-iron (Fe). At high gradients, the saturation within the cores plays a major role, but simulations get more complex due to the steep magnetization curve of CoFe.

For the built setup the calculated fill factor is about 67 %, which is a realistic value for hand-wound coils. The result for a larger current, where saturation effects come into play, can be seen in Figure 2. The profile of the magnitude of the flux density still match very well for the field on the y-axis as well as on the x-axis. Thus, the simulation correctly reproduces the field together with the saturation properties of the soft-iron. Deviations between simulation and measurement can be due to the fact that both coils could have different filling factors. Furthermore, the slope of the measurement is limited by the number of measurement points. Here, fields with a maximum polynomial degree of 6 can be reproduced exactly. This can be a reason why the drop of the field at the edges of the x-axis is not fully visible in the measurement.

The power consumption of the system for FFPs on the y-axis is shown in the third plot in Figure 2. In contrast to MPI scanners in standard coil configuration, the power consumption of the system is decreased when the FFP moves to one of the coil arrays. This is due to the fact that the coils can enter a single-sided mode in which far away coils only need to be supplied with very low currents. Additionally, the array-shaped coil arrangement allows to shift the FFP with only a comparatively small increase in power in the other directions.

IV. Conclusion

In this work, an optimized high field iron SeFo generator has been presented. FFP positions inside a $10 \times 8 \times 10\,\mathrm{cm}^3$ volume with gradients of more than $1.5\,\mathrm{Tm}^{-1}$ are accessible. The overall power consumption for field generation is in a range, which still allows air cooling. Due to the array-shaped coil assembly, flexible field values are possible for every position. This enables new possibilities for force experiments together with simultaneous imaging. Additionally, the nonlinear inverse current problem can be studied in detail, which has to be handled properly for human-sized MPI scanner.

Author's statement

Research funding: The authors thankfully acknowledge the financial support by the German Research Foundation (DFG, grant number KN 1108/7-1 and GR 5287/2-1) and the Federal Ministry of Education and Research (BMBF, grant number 05M16GKA). Conflict of interest: Authors state no conflict of interest.

References

[1] J. Rahmer, C. Stehning, and B. Gleich. Remote magnetic actuation using a clinical scale system. *PLOS ONE*, 13(3):e0193546, 2018, Publisher: Public Library of Science. doi:10.1371/journal.pone.0193546.

[2] M. Graeser, F. Thieben, P. Szwargulski, F. Werner, N. Gdaniec, M. Boberg, F. Griese, M. Möddel, P. Ludewig, D. van de Ven, O. M. Weber, O. Woywode, B. Gleich, and T. Knopp. Human-sized magnetic particle imaging for brain applications. *Nature Communications*, 10(1):1936, 2019, doi:10.1038/s41467-019-09704-x.

[3] E. E. Mason, C. Z. Cooley, S. F. Cauley, G. A Mark, S. M. Conolly, and L. L. Wald. Design analysis of an MPI human functional brain scanner. *International Journal on Magnetic Particle Imaging*, Vol.3:12 pages, 2017, Artwork Size: 12 pages Publisher: Infinite Science Publishing. doi:10.18416/IJMPI.2017.1703008.

[4] F. Thieben, M. Boberg, P. Szwargulski, M. Graeser, and T. Knopp. Gradient power reducing using pulsed selection-field sequences. *International Journal on Magnetic Particle Imaging.*, 6(2):1–3, 2020, inproceedings. doi:10.18416/IJMPI.2020.2009054.

[5] K. Sajjamark, J. Franke, H. Lehr, R. Pietig, and V. Niemann. Spatial selectivity enhancement in magnetic fluid hyperthermia by magnetic flux confinement. *International Journal on Magnetic Particle Imaging*, pp. Vol 7 No 1 (2021), 2021, Publisher: International Journal on Magnetic Particle Imaging. doi:10.18416/IJMPI.2021.2103002.

[6] A. C. Bakenecker, J. Schumacher, P. Blümler, K. Gräfe, M. Ahlborg, and T. M. Buzug. A concept for an mpi scanner with halbach arrays. *International Journal on Magnetic Particle Imaging*, pp. Vol 6 No 2 Suppl. 1 (2020), 2020.

[7] F. Griese, P. Ludewig, C. Gruettner, F. Thieben, K. Müller, and T. Knopp. Quasi-simultaneous magnetic particle imaging and navigation of nanomag/synomag-D particles in bifurcation flow experiments. *International Journal on Magnetic Particle Imaging*, pp. Vol 6 No 2 Suppl. 1 (2020), 2020, Publisher: International Journal on Magnetic Particle Imaging. doi:10.18416/IJMPI.2020.2009025.

[8] A. C. Bakenecker, A. von Gladiss, T. Friedrich, U. Heinen, H. Lehr, K. Lüdtke-Buzug, and T. M. Buzug. Actuation and visualization of a magnetically coated swimmer with magnetic particle imaging. *Journal of Magnetism and Magnetic Materials*, 473:495–500, 2019, doi:10.1016/j.jmmm.2018.10.056.

[9] F. Foerger, M. Graeser, and T. Knopp. Iron core coil designs for MPI. *International Journal on Magnetic Particle Imaging*, 6(2):1–3, 2020, doi:10.18416/IJMPI.2020.2009042.

[10] M. Boberg, T. Knopp, and M. Möddel. Analysis and comparison of magnetic fields in MPI using spherical harmonic expansions. *8th International Workshop on Magnetic Particle Imaging (IWMPI 2018)*, pp. 159–160, 2018, inproceedings.

